DEFENSE TECHNICAL INFORMATION CENTER

Information for the Defense Community

DTIC® has determined on ⨯ 1/8 l2O/l2 that this Technical Document has the Distribution Statement checked below. The current distribution for this document can be found in the DTIC® Technical Report Database.

☒ **DISTRIBUTION STATEMENT A.** Approved for public release; distribution is unlimited.

☐ **© COPYRIGHTED**; U.S. Government or Federal Rights License. All other rights and uses except those permitted by copyright law are reserved by the copyright owner.

☐ **DISTRIBUTION STATEMENT B.** Distribution authorized to U.S. Government agencies only (fill in reason) (date of determination). Other requests for this document shall be referred to (insert controlling DoD office)

☐ **DISTRIBUTION STATEMENT C.** Distribution authorized to U.S. Government Agencies and their contractors (fill in reason) (date of determination). Other requests for this document shall be referred to (insert controlling DoD office)

☐ **DISTRIBUTION STATEMENT D.** Distribution authorized to the Department of Defense and U.S. DoD contractors only (fill in reason) (date of determination). Other requests shall be referred to (insert controlling DoD office).

☐ **DISTRIBUTION STATEMENT E.** Distribution authorized to DoD Components only (fill in reason) (date of determination). Other requests shall be referred to (insert controlling DoD office).

☐ **DISTRIBUTION STATEMENT F.** Further dissemination only as directed by (inserting controlling DoD office) (date of determination) or higher DoD authority.

Distribution Statement F is also used when a document does not contain a distribution statement and no distribution statement can be determined.

☐ **DISTRIBUTION STATEMENT X.** Distribution authorized to U.S. Government Agencies and private individuals or enterprises eligible to obtain export-controlled technical data in accordance with DoDD 5230.25; (date of determination). DoD Controlling Office is (insert controlling DoD office).

AFRL-RV-HA-TR-2008-1129

Compact Environmental Anomaly Sensor (CEASE): Geometric Factors

Donald Brautigam

04 Nov 2008

AIR FORCE RESEARCH LABORATORY
AIR FORCE MATERIEL COMMAND
Space Vehicles Directorate
29 Randolph Rd.
Hanscom AFB, MA 01731-3010

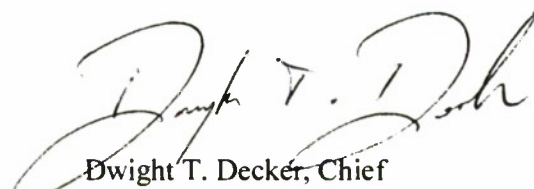20100201217

AFRL-RV-HA-TR-2008-1129

This technical report has been reviewed and is approved for publication.

Robert A. Morris, Director
Battlespace Environment Division

James I Metcalf
Project Scientist

Dwight T. Decker, Chief
Space Weather Center of Excellence

REPORT DOCUMENTATION PAGE

Public reporting burden for this collection of information is estimated to average 1 hour per response, including the time for reviewing instructions, searching existing data sources, gathering and maintaining the data needed, and completing and reviewing this collection of information. Send comments regarding this burden estimate or any other aspect of this collection of information, including suggestions for reducing this burden to Department of Defense, Washington Headquarters Services, Directorate for Information Operations and Reports (0704-0188), 1215 Jefferson Davis Highway, Suite 1204, Arlington, VA 22202-4302. Respondents should be aware that notwithstanding any other provision of law, no person shall be subject to any penalty for failing to comply with e collection of information if it does not display e currently valid OMB control number. **PLEASE DO NOT RETURN YOUR FORM TO THE ABOVE ADDRESS.**

1. REPORT DATE (DD-MM-YYYY)	2. REPORT TYPE		3. DATES COVERED (From - To)
04-11-2008	Scientific, Final		Scientific, Interim

4. TITLE AND SUBTITLE	5a. CONTRACT NUMBER
Compact Environmental Anomaly Sensor (CEASE) : Geometric Factors	N/A
	5b. GRANT NUMBER N/A
	5c. PROGRAM ELEMENT NUMBER PE 62601F

6. AUTHOR(S)	5d. PROJECT NUMBER
D. Brautigam	1010
	5e. TASK NUMBER RS
	5f. WORK UNIT NUMBER A1

7. PERFORMING ORGANIZATION NAME(S) AND ADDRESS(ES)	8. PERFORMING ORGANIZATION REPORT NUMBER
Air Force Research Laboratory 29 Randolph Rd. Hanscom AFB, MA 01731-3010	AFRL-RV-HA-TR-2008-1129

9. SPONSORING / MONITORING AGENCY NAME(S) AND ADDRESS(ES)	10. SPONSOR/MONITOR'S ACRONYM(S)
	AFRL/RVBXR
	11. SPONSOR/MONITOR'S REPORT NUMBER(S)

12. DISTRIBUTION / AVAILABILITY STATEMENT

Approved for public release; distribution unlimited.

13. SUPPLEMENTARY NOTES

14. ABSTRACT

A previously published technical report [AFRL-VS-HA-TR-2006-1030] was the first in a series by AFRL to document the performance of the Compact Environmental Anomaly Sensor (CEASE). That report includes (1) a definition of the response function and its relation to the geometric factor; (2) a description of the Monte Carlo simulations that were performed to determine the proton and electron response functions for the telescope and dosimeters; and (3) the resulting response functions and a comparison with experimental calibration results. This report details how these response functions are used to estimate a set of geometric factors for a set of integral flux channels derived for both the telescope and dosimeters.

15. SUBJECT TERMS Compact environmental anomaly sensor, CEASE, Detector response functions, Geometric factors

16. SECURITY CLASSIFICATION OF:			17. LIMITATION OF ABSTRACT	18. NUMBER OF PAGES	19a. NAME OF RESPONSIBLE PERSON
a. REPORT UNCLASSIFIED	**b. ABSTRACT** UNCLASSIFIED	**c. THIS PAGE** UNCLASSIFIED	UNL	24	Gregory P. Ginet **19b. TELEPHONE NUMBER** (include area code)

Table of Contents

Figures

1. INTRODUCTION

A previously published technical report [Brautigam, et al., 2006; hereafter referred to as TR#1] was the first in a series by AFRL to characterize the response of the Compact Environmental Anomaly Sensor (CEASE). That report (TR#1) includes (1) a definition of the response function and its relation to the geometric factor; (2) a description of the Monte Carlo simulations that were performed to determine the proton and electron response functions for the telescope and dosimeters; and (3) the resulting response functions and a comparison with experimental calibration results. This report details how these response functions are used to estimate a set of geometric factors for a set of integral flux channels derived for both the telescope and dosimeters.

As described in TR#1, CEASE includes a telescope and two dosimeters (thin shield, DD1; thick shield, DD2). The telescope includes a front (DFT) and back (DBT) solid state detector. A particle passing through the telescope will deposit some portion of its incident energy (either 0 or some non-zero fraction) in each of the 2 detectors. The energy deposition scale for each of DFT and DBT is divided into 9 intervals so that the pair of detectors leads to 81 (9 x 9) different logic blocks designated by LB(I,J), where I and J label the energy deposition interval for DBT and DFT, respectively. Various groups of adjacent logic blocks are summed on board the satellite to reduce telemetry demands. Each dosimeter (DD1 and DD2) has three Linear Energy Transfer (LET) channels defined by the energy deposition range in the dosimeter's single solid state detector, which for CEASE sn002, are the following: LoLET (0.05 – 0.8 MeV), HiLETA (0.8 - 3.0 MeV) and HiLETB (3.0-10. MeV), for both flux count rates and dose count rates. For CEASE sn007, the energy deposition boundary between LoLET and HiLETA channels is 1.0 MeV instead of 0.8 MeV. The telescope logic block channels (individual or summed) and the dosimeter channels that are included in the telemetry stream are listed in Appendix A.

2. CEASE GEOMETRIC FACTORS

An isotropic differential flux spectrum $j(E)$ is related to the ith channel count rate C_i according to the following integral, where $R_i(E)$ is the energy dependent response function for the ith channel:

$$C_i = \int_0^\infty R_i(E) j(E) dE \tag{1}$$

A consistent set of units for the above variables are: C_i [counts/s], $R_i(E)$ [cm^2 sr], E [MeV], and $j(E)$ [#/(cm^2 s sr MeV)]. In the case where $R_i(E)$ can be approximated by a step function with an energy threshold E_T and constant non-zero value $R_i(E) = G_i$ for $E > E_T$, (1) can be simplified to:

$$C_i = G_i \int_{E_T}^\infty j(E) dE \tag{2}$$

With the definition of integral flux $J_{>E_T} \equiv \int_{E_T}^\infty j(E) dE$, Eq. (2) reduces to:

$$J_{E_T} = \frac{C_i}{G_i} \tag{3}$$

1

In the case where $R_i(E)$ can be approximated by a constant non-zero value (g_i) within a relatively narrow energy interval $[E_1, E_2]$ throughout which $j(E) \sim j_i$ = constant, then Eq. (1) reduces to $C_i = j_i g_i \Delta E$ and the differential flux for the ith channel [with $E=(E_1+E_2)/2$; $\Delta E_i = E_2 - E_1$] is given by:

$$j_i(E) = \frac{C_i}{g_i \Delta E_i} \tag{4}$$

where $j(E)$ is a differential flux in units of $(cm^2 \ s \ sr \ MeV)^{-1}$.

In principle, given a set of channel count rates and response functions, one can invert the set of corresponding integral equations Eq. (1) to solve for the unknown differential flux. However, in practice this is problematic because one typically is faced with an "ill-conditioned" set of equations whose solution is very unstable to small variations in the known quantities, often leading to unphysical results. Successful inversion methods must therefore constrain the solution by various assumptions based on physicality. The more expeditious (though less accurate) technique utilized in routine data processing, and the focus of this report, employs the concept of a geometric factor using the approximate relation given by Eq. (3) for integral flux. In the following we define a set of telescope and dosimeter channels with geometric factors from which one may compute approximate integral fluxes.

A complicating factor in using any of the above algorithms to derive a flux spectrum from a set of channel count rates is that many of the channels respond to both electrons and protons. Any contribution to the measured count rate by unwanted background will introduce an error in the inferred spectrum. If one can specify the background spectrum it is possible to mitigate this source of error by applying some form of background subtraction algorithm, although this will not be addressed in this report. Fortunately, except during the relatively rare time when there is a solar proton event in progress, the outer zone belt is essentially free of energetic protons that could produce a background signal in the "electron channels." Although the inner zone is comprised of both protons and electrons, there are some "proton channels" that have very small, if any, electron response.

TR#1 describes in detail the method by which individual response functions $R_i(E)$ were determined for telescope and dosimeter channels listed in Appendix A. In that report, Figures 13 (for protons) and 15 (for electrons) illustrate that the individual telescope $R_i(E)$ are poor approximations of either narrow Gaussians or step functions, and therefore are not appropriate for estimating either differential flux (through Eq. (3)) or integral flux (through Eq. (4)). However, in many cases summing the response for several channels yields a resultant $R(E)$ that better approximates a step function over a limited energy range where the expected particle flux is most intense and contributes most significantly to the integral in Eq. (1). Such combined channels where a number of individual logic block channels have been summed to give a new set of "standard" telescope channels T1-T4 are given in Appendix B. Appendix C.1 lists the full set of standardized flux channels (labeled in the first column) from the dosimeters (D1-D8) and the telescope (T01-T09) for TSX5 (CEASE sn002). The second column describes which instrument channel(s) are associated with the standard channel label. The electron channel response is defined by an energy threshold E_T (column 3) and geometric factor G (column 4); the proton channel response is defined by E_T (column 5) and G (column 6). An analogous table exists for DSP21 (CEASE sn007) in Appendix C.2), and DSX (CEASE sn004) in Appendix C.3.

2

The tabulated geometric factors were determined using two different methods referred to here as the Bow Tie Analysis [*Van Allen et al., 1974*] and a modified Bow Tie Analysis. Both methods use the following relation (from Eqs. (1) and (2), where $R_i(E)$ is the response function for the ith channel from the set D01-D08 or T01-T09 :

$$G_i = \frac{\int_0^\infty R_i(E)j(E)dE}{\int_{E_T}^\infty j(E)dE} \tag{5}$$

Given $R_i(E)$, one can solve for G_i by assuming a form of $j(E)$ and an energy threshold E_T. If $R_i(E)$ were an exact step function (with step at E_T) then this relation would be an equivalence independent of the spectral form of $j(E)$. Since this is not the case, its dependence on both the spectral shape of $j(E)$ and E_T introduces significant uncertainty in the definition of G_i. To the degree that the ramp-up of the real response deviates from a step function, the value of G determined from Eq. (5) will be sensitive to the chosen value of E_T. Also, the fact that the value of G_i is dependent upon the spectral shape of the measured flux distribution is obviously problematic given that the spectral shape may vary over space and time.

The Modified Bow Tie Analysis (MBTA) is described first since this was the approach first taken. The MBTA assumes a predetermined range of spectral shape index (γ) as well as its most probable value and determines the corresponding values of E_T using a technique described below. It then computes G using Eq. (5) for each of the three pairs of (γ, E_T). An uncertainty in G_i may be inferred from the lower and upper limit of G (G_L and G_U, respectively).

The range of spectral shape index (γ) was inferred by the differential flux spectra defined by CRRES instrumentation (PROTEL for protons; MEA and HEEF for electrons) which had superior energy and angular resolution relative to the CEASE instrumentation. These results are provided in detail in Appendix D.1 (protons) and D.2 (electrons), and are summarized here. For both electrons and protons, the CRRES fluxes were fit to both power law ($j \sim E^{-n}$) and exponential ($j \sim \exp(-E/E_o)$) spectral shapes, with spectral indices $\gamma = n$ and $\gamma = E_o$, respectively . It was found that throughout the inner zone (L = 1.4 – 2), the protons were best characterized by a power law spectrum with n = 1 to 4, with n ~ 2 at the heart of the belt (L ~ 1.5). These CRRES results were in relatively good agreement with AP8 results. Solar proton spectra may typically be characterized by power laws with n ~ 2-3 [*Kahler, 2006*]. Throughout the outer zone, electron spectra were found to be best characterized by an exponential spectrum, although as L ~ 6.6 (geosynchronous) is approached from lower L, power laws gave a marginally better fit. The average characteristic energy E_o is ~ 0.35 MeV for L = 3-4 and decreases to ~ 0.2 MeV for L = 5-6. The average E_o for L = 3-6 is ~ 0.3 MeV with a range of ~ 0.1 to 0.5 MeV.

The energy threshold E_T for any given R(E) and γ is based on the following parameter computed as a function of E (upper endpoint of the numerator's integral):

$$\delta(E_T) = \frac{\int_0^{E_T} R(E')j(E')dE'}{\int_0^\infty R(E')j(E')dE'} \tag{6}$$

This is the fraction of the total count rate that is attributed to the flux below a specified energy E. The energy threshold E_T is chosen to be that energy for which $\delta(E)$ first reaches (or exceeds) the threshold value of 0.1. This critical value of δ is chosen somewhat arbitrarily, though it provides a quantifiable criterion for defining E_T that can be consistently applied to all channel responses.

3

The geometric factor G_i for the ith channel is thus determined using a specified spectral index to define the differential flux j(E) in (5), and a threshold energy E_T determined by analyzing the function $\delta(E)$ described above. Results using this procedure are illustrated in Figure 1 for sample channels.
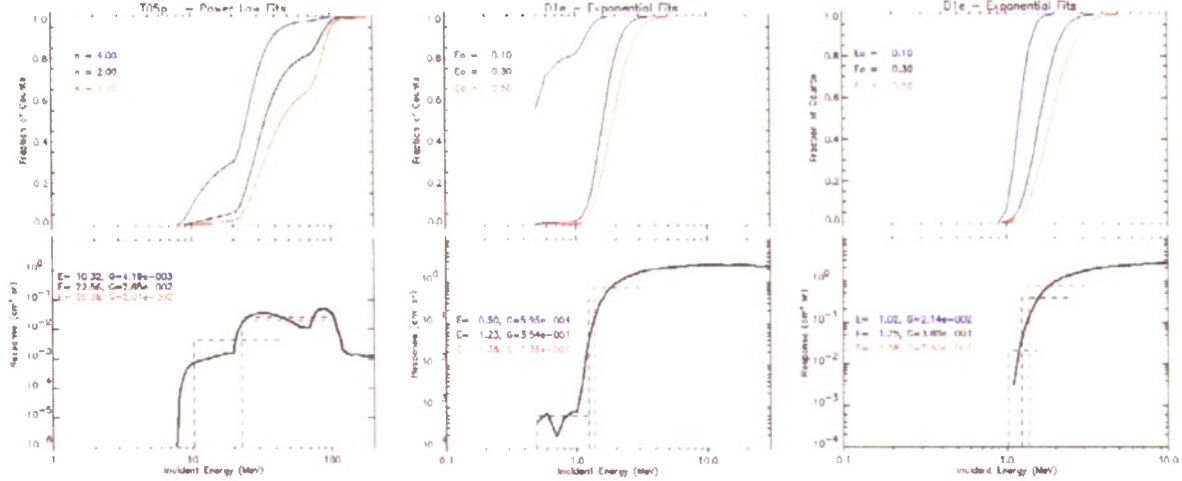

Fig. 1 Results of geometric factor computation for proton response to channel T5 (left panels), and electron response to channel D1 (middle and right panels). Top panels plot $\delta(E)$ vs E and bottom panels plot G and R(E) vs E. The colored solid curves for δ (top) and the colored dashed curves for G (bottom) correspond to different spectral indices (key in top panels) and threshold energies E_T (key in bottom panels). The red curves correspond to relatively hard spectral index (low n, high E_o); the blue curves, to relatively soft spectral index (high n, low E_o); and the black curves, to the more typical spectral index as determined by a survey of CRRES and NASA spectra.

The channel T05 proton response illustrates the sensitivity of the results to the spectral hardness. For the power law n = 4 (soft, steeply falling spectrum) a substantial fraction of the counts come from the lowest energy portion of the response curve. Because the response for T5 is "two-tiered," the computed E_T and G for n = 1.1 and 2 spectra, which are relatively flat and weight more heavily the higher energy portion of the response curve, are significantly larger than that for the n = 4 spectrum. The middle panels illustrate the electron response to the D1 channel. The response curve (bottom panel) shows a fairly ragged response below 1 MeV which is attributed to a weak bremsstrahlung signal with relatively poor statistics and does not correspond to the penetration of primary electrons. For the exponential $E_o = 0.1$ MeV (soft, steeply falling spectrum) about 80% of the counts arise from this part of the response curve. This result is compared to the rightmost panels which show the analogous results for D1 where the bremsstrahlung response is neglected. For very soft spectra the uncertainty in E_T and G can be greatly compounded by the noise level near the "turn-on" point of the response curves.

The deviation of some of the response curves from an ideal step function is so great that they are worthless in terms of integral channels. Figure 2 illustrates such channels. Channel D02 has a proton response with such a gradual ramp that the uncertainty of E_T is too great to be useful. Channel T02 has a proton response at ~ 1 MeV, a broad minimum in response between 1.5 and 15 MeV, and then a ramping up to its maximum response. Channel T06 has no detectable electron response below ~5 MeV and does not flatten until beyond 10 MeV which is past the energy range of practical interest. For channels such as these, a lower energy is listed in the Appendix C tables but the value of G is labeled N/A (Not Applicable) because no reasonable G could be computed.

4

Channel T07 (not shown) responds to protons with very wide incident angles, missing the front detector but penetrating the back detector. It has become evident that modeling channel T07 is problematic since many of the contributing protons penetrate the spacecraft walls far from the telescope cover. Therefore, the range of incident angle has been restricted to 0° to 45° and channel T07 is ignored. Ignoring incident angles greater than 45° introduces a small error which is relatively negligible compared to the other uncertainties discussed.

Figure 2. Shown here (left to right) in a format identical to Figure 1 is the proton response for channels D02 and T02, and the electron response for T06.

As illustrated by Figure 3, the summation of the dosimeter LoLET and HiLETA channel proton responses result in a much better approximation to a step function then either one by themselves.
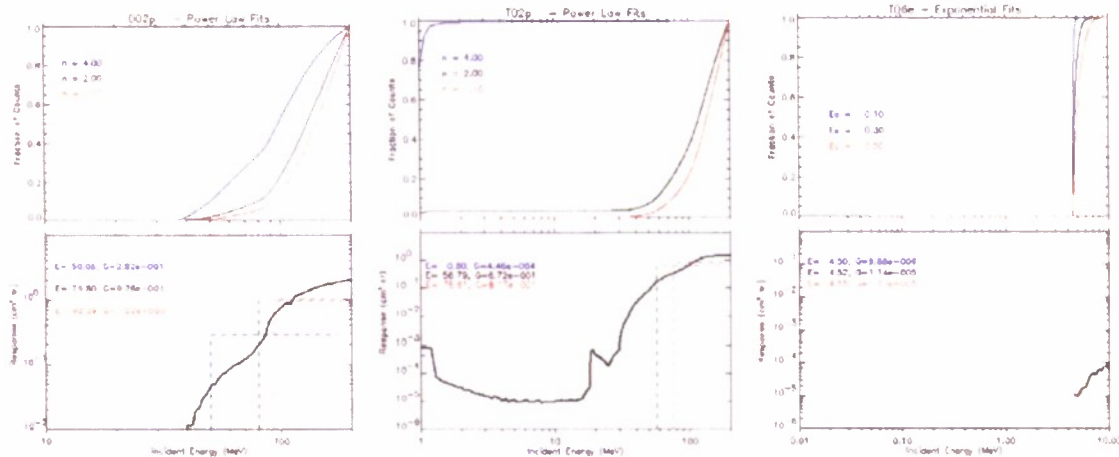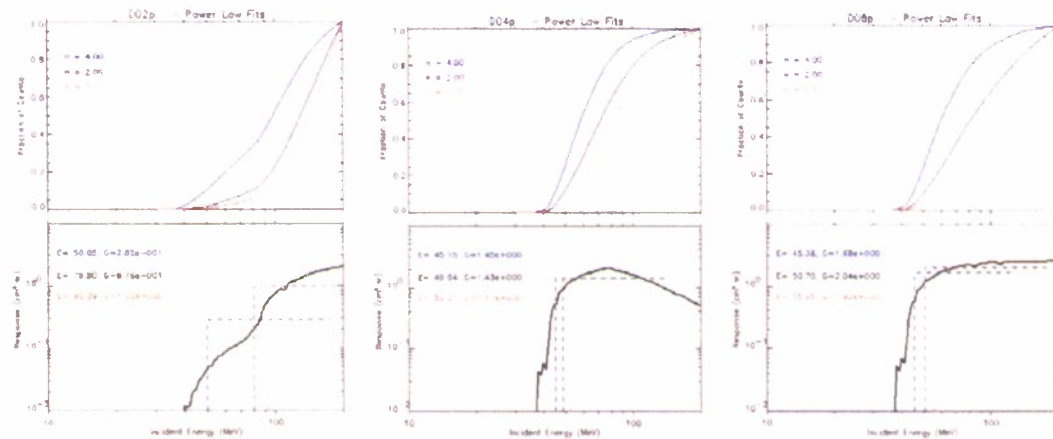

Figure 3. Shown here (left to right) in a format identical to Figure 1 is the proton response for channels D02, D04, and the sum of D02 plus D04 (= D08).

A second method that may be used to compute the geometric factors is the Bow Tie Analysis (BTA). This method also utilizes equation (5) but is based on a graphical technique for its solution.

5

Using a predetermined range of the spectral index (γ) and threshold energies (E_T), several curves parameterized by γ, $G(E_T; \gamma)$, are computed and plotted as illustrated in Figure 4 where BTA is used to determine (E_T, G) for electron dosimeter channel D02 assuming exponential spectra.
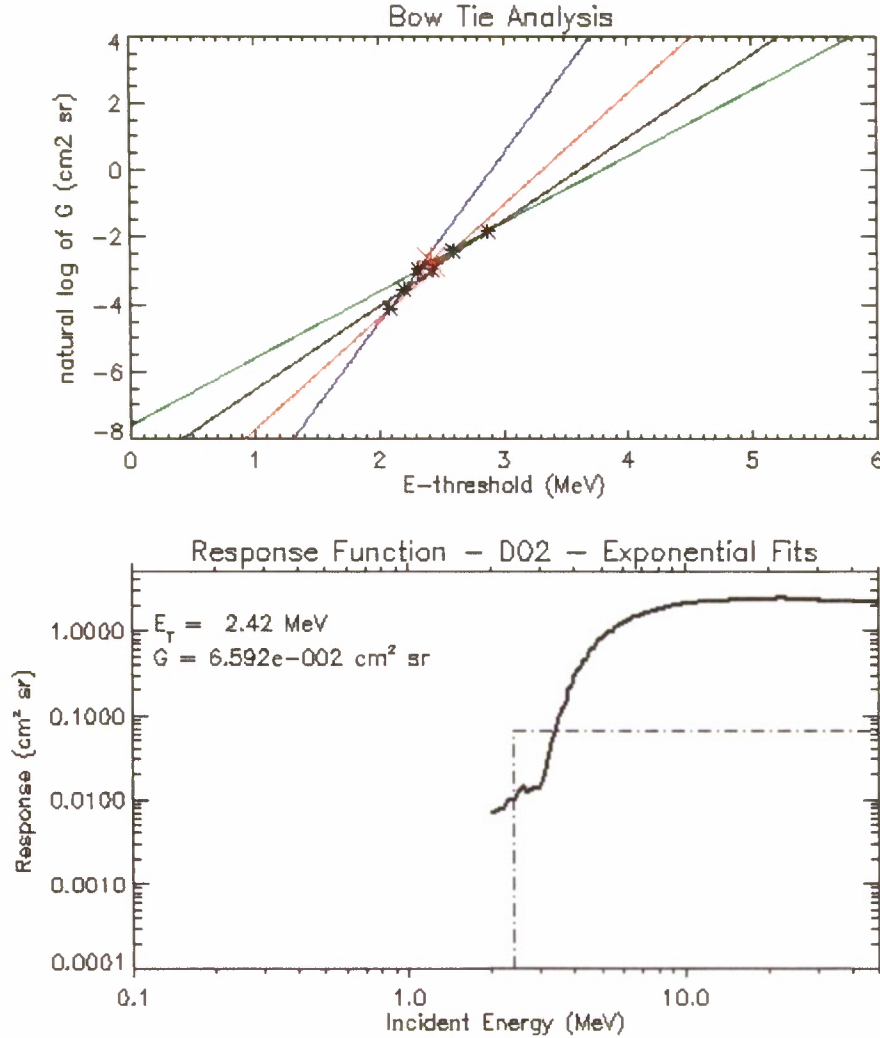
Figure 4. Bow Tie Analysis for TSX dosimeter electron channel D02. The colored lines (top panel) are parameterized by γ. For the electron exponential fits shown here, $\gamma = E_o = 0.2$ (blue), 0.3 (red), 0.4 (black), and 0.5 (green). The point marked by the red asterisk in the top panel corresponds to the threshold energy (E_T) and geometric factor (G) designated on the response function plot (lower panel).

The values of E_T and G correspond (ideally) to the "point" in the upper plot where the parameterized lines converge. In practice, as Figure 4 illustrates, the "point" of convergence is generally quite spread out and underscores the obvious source of uncertainty in this method. The stated values have been determined by an algorithm that determines the coordinates of all the points of intersection between the various pairs of lines. The E coordinates and G coordinates are then separately averaged (and their standard deviation determined) to give the solution (E_T, G) which is

then listed and plotted (with dashed lines) on the plot of the response function (lower panel). One has the option of weighting the various lines according to the probability of encountering spectra with the corresponding spectral index, but this is not done here. It should also be pointed out that whereas the BTA is able to define (E_T, G) for D02, the MBTA is not unless the bremsstrahlung contribution at the lowest energies (<3 MeV) is ignored.

Another point to emphasize in comparing the results between MBTA and BTA, is that the range of solutions from BTA depends upon the range of spectral index is used. In Figure 5 the results for the telescope proton channel T05 are shown. The left panel, where the 4 power law indices used are {1.1 (green), 2.0 (black), 3.0 (red), and 4.0 (blue)}, shows a resulting $E_T = 11.5$ MeV. The right panel, where n = 1.1 has been excluded, shows a resulting $E_T = 16.3$ MeV. These results may be compared with result from Figure 1 (left panel) where MBTA gives $E_T = 22.6$. These differences underscore the point that although it is more convenient to have a specific energy and geometric factor assigned to each individual channel, there are many arguments to be made for utilizing the full response function and inferring a flux spectrum through some inversion algorithm.
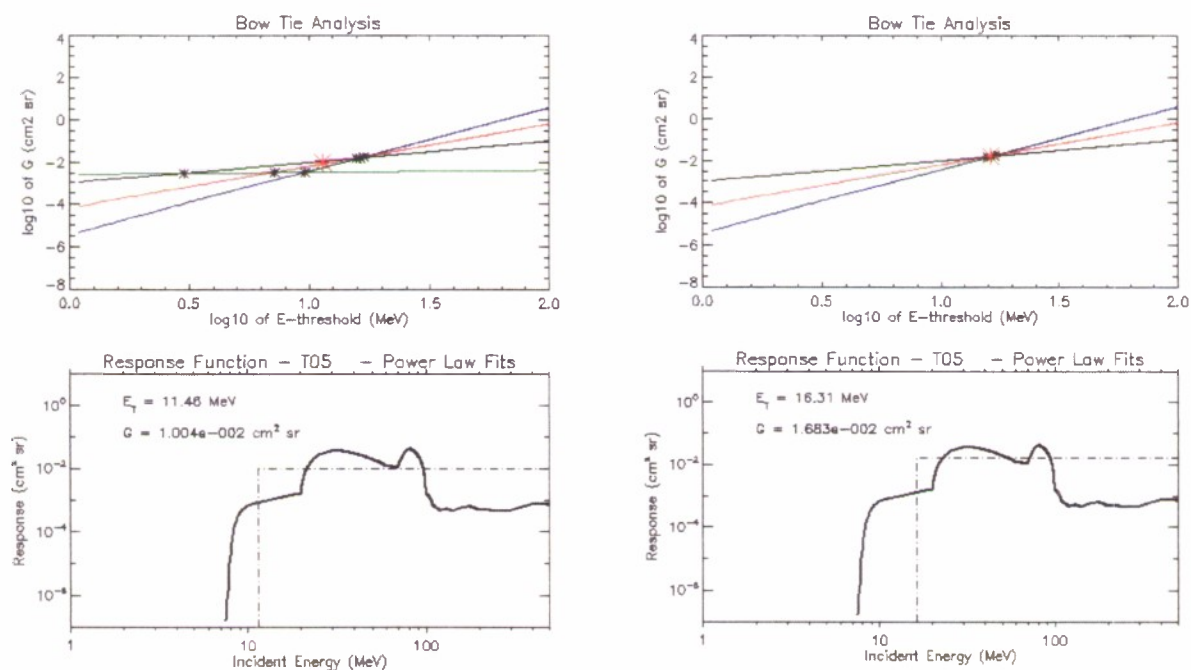
Figure 5. Comparison of Bow Tie Analysis assuming 4 spectral indices (left) and 3 spectral indices (right) for telescope proton channel T05.

The results of both BTA and MBTA are summarized in Appendix C. Whereas the results illustrated in the Figures 1 to 3 are based on the earlier used upper limit energies for electrons (10 MeV) and protons (200 MeV), the final results in Appendix C are based on revised upper limit energies for electrons (50 MeV) and protons (500 MeV) – hence, there may be differences in results quoted here as compared to previous results.

3. SOFTWARE DOCUMENTATION

An individual Monte Carlo (MC) run (MCNPX or ACCEPT) is made for each pair of incident particle energy (E) and angle (θ), each run consisting of thousands of particle trajectories whose entry point from the designated source surface area is randomly chosen. For each of these runs, an "input deck" is generated that consists of the instrument geometry and material list (this part is the same independent of the source energy/angle and is read in as a standard file), followed by several lines which define the source characteristics and the format of the output files (these lines are generated by the Monte Carlo "run" software). To automate the process of making hundreds of individual runs and to facilitate the post-MC-run data processing and bookkeeping task, a number of auxiliary software programs were developed. The various geometry files used for creating the "input decks" are summarized in Table 1. The specific programs for running the Monte Carlo codes (MCNPX and ACCEPT) and performing post-MC analysis are summarized in Table 2.

Table 1. Input Deck Geometry Files.[1]

Sat	Inst/ specie	Geometry File (c:\science\...)	Description	Input to: (see Table 2)
TSX-5	Tele / e	ACCEPT\geometry\TEL-TSX_accept_geometry_v00.txt	Bare telescope	run_accept_tele.for
		ACCEPT\geometry\TEL-TSX_accept_geometry_v01.txt	In frame/case	
DSP21	Tele / e	ACCEPT\geometry\TEL-DSP_accept_geometry_v00.txt	Bare telescope	run_accept_tele.for
		ACCEPT\geometry\TEL-DSP_accept_geometry_v01.txt	In frame/case	
DSX	Tele / e	ACCEPT\geometry\TEL-DSX_accept_geometry_v00.txt	Bare telescope	run_accept_tele.for
		ACCEPT\geometry\TEL-DSX_accept_geometry_v01.txt	Not used	
All	Dose / e	ACCEPT\geometry\DD-accept_geometry_v01.txt	DD1&DD2 in case	run_accept_dose.for
TSX-5	Tele / p	mcnpx\geometry\TEL-TSX_mcnpx_geometry_v00.txt	In case	run_mcnpx_tele.for
DSP21	Tele / p	mcnpx\geometry\TEL-DSP_mcnpx_geometry_v00.txt	In case	run_mcnpx_tele.for
DSX	Tele / p	mcnpx\geometry\TEL-DSX_mcnpx_geometry_v00.txt	Tele;DD1;DD2 in case	run_mcnpx_tele.for
All	Dose/ p	mcnpx\geometry\DOS_mcnpx_geometry_v00.txt	DD1; DD2 in case w/ tele cyl	run_mcnpx_dose.for

---

1

8

Table 2. Auxiliary software for Monte Carlo analysis.

Code Name	Folder Location (c:\science\...)	Description
run_mcnpx_tele.for	mcnpx\mcnpx_exe\	Runs either species, any satellite, for telescope – runs mcnps.exe, and outputs p_DSX_E003000_A00_v03_lbm.txt, etc
run_accept_tele.for	Accept\accept_cease_tele\	Runs electrons, any satellite, for telescope – runs accsng1.exe, outputs e_TSX_E001000_A00_lbm.txt, etc
response_tele.for	Response_code\	Reads input files (various versions and formats depending who created them) – for either species and any satellite and outputs eResponse_DSP_tel.txt, eAngularR_DSP_tel.txt, etc
plot_tele_response.pro	Response_code\	Reads output from response_tele.for – either species and any satellite, and plots response for channels; produces listing for standard channel responses
run_mcnpx_dose.for	mcnpx\mcnpx_exe\	Runs for either species, for dosimeter– runs mcnpu, and outputs p_dos_E044000_A00_v01_tbl.txt, etc Same output used for any satellite
response_mcnpx_dose.for	Response_code\	Reads in output from run_mcnpx_dose.for, creates LoLET, HiLETA, and HiLETB channel table for both domes
run_accept_dose.for	accept\accept_cease_dose\	Runs for electrons, for dosimeter– runs accJ16.exe, and outputs e_DOS_E044000_A00_v01_out.txt, etc Same output used for any satellite
response_accept_dose.for	Response_code\	Reads in output from run_accept_dose.for, outputs DD_SN2_eResponse.txt and DD_SN4_eResponse.txt (all channels, both dosimeters – for both TSX5 and DSP21 (=DSX); also separate files for separate domes: DD1(2)_SN2_eResponse.txt, etc
plot_dose_response.pro	Response_code\	Reads dosimeter output – either species and any satellite, and plots response for channels
geometric_factor.pro	Response_code\	Does modified Bow Tie Analysis; outputs plots and tables
bowtie.pro	Response_code\	Does Bow Tie Analysis; outputs plots

9

The program run_mcnpx_tele.for is designed to flexibly handle a variety of cases. The user must specify the CEASE satellite (isat), particle species (ispecies), and version number (iver) which may vary depending upon (for example) the source definition or executable version used. The set of energies and angles to be run are specified by an input file *sat_p*_energies_v*xx*.txt, where *sat* is a 3-letter identifier for the satellite (*TSX, DSP, DSX*); *p* is a single-letter identifier for particle species (*p* for proton; *e* for electron), and xx is a 2-digit identifier for version number. This file is formatted with the number of energies on the first line, followed by the set of energies; and then the number of angles, followed by the set of angles. The program loops through sets of energies and angles, and for each (E,θ) executes the appropriate code depending on what flags are set. If the *imcnpx* flag is set, the relevant instrument geometry file is read in and, along with specific particle source information, the MCNPX input deck is generated. MCNPX is then executed producing its standard OUTPUT file. If the *iconvert* flag is set, then the OUTPUT file for specified (isat,ispecies,iver,E,θ) is read through and only the essential information (number of histories, incident energy and angle, probability distribution P(E,θ), average energy deposition per specified cell, etc) is extracted and written to an auxiliary file. At this point the P(E,θ) is specified for each logic channel (for the telescope there are 9 DFT x 9 DBT = 81 logic channels). The *imcnpx* and *iconvert* are independent so that all OUTPUT files may be generated first and then at a later time may be converted. The file naming convention used for the CEASE telescope is the following:

s_SAT_Eeeeeee_Aaa_Vvv_in.txt - (INPUT file)
s_SAT_Eeeeeee_Aaa_Vvv_out.txt – (OUTPUT file)
s_SAT_Eeeeeee_Aaa_Vvv_tbl.txt – (table of individual history outcomes)
s_SAT_Eeeeeee_Aaa_Vvv_lbm.txt – (summary table of logic block matrix of P(E,θ) results)

The first character specifies the species (s = p, proton; e, electron); SAT species the satellite (SAT = TSX, DSP, DSX, NRL); eeeeee specifies the energy E in keV; aa specifies the angle A in degrees; and vv specifies the version V. All numerical labels are padded with leading zeros.

The logic for run_accept_tele.for is similar to that for run_mcnpx_tele.for, though there are some differences. In particular, the ACCEPT codes require that cross-section tables be generated for each energy, and this is accomplished with run_accept_tele.

Once the logic channel P(E,θ) data are written, a second program (response_tele.for) can be run which reads in P(E,θ) and computes for the subset of telemetry channels the energy and angle dependent effective area A(E,θ). Some telemetry channels are the individual logic block channels, whereas some are summations of two or more individual logic channels which have been combined because of their similar response and to conserve on telemetry. Another file is written that includes the energy-dependent response $R(E) = 2\pi \int_0^{\pi/2} A(E,\theta) \sin\theta d\theta$ (see Table 2 for sample naming conventions).

REFERENCES

Brautigam, D.H., et al., "Compact Environmental Anomaly Sensor (CEASE): Response Functions," AFRL-VS-HA-TR-2006-1030, March 2006.

Kahler, 2006. private communication.

Van Allen, J., et al., JGR, 79, 3559, 1974.

APPENDIX A – PRIMARY TELESCOPE AND DOSIMETER CHANNELS

CEASE / Telescope				CEASE / Dosimeter	
data ch#	channel	data	channel	data	Channel
01	LB(1,0)	21[3]	LB-SUMA	01	DD1-LoLET-Flux (DD1LF)
02	LB(2,0)	22[4]	LB-SUM1	02	DD1-HiLETA-Flux (DD1HFA)
03	LB(3,0)	23[5]	LB-SUM2	03	DD1-HiLETB-Flux (DD1HFB)
04	LB(4,0)	24[6]	LB-SUMB	04	DD1-LoLET-DRC (DD1LD)
05	LB(5,0)	25[7]	LB-SUM3	05	DD1-HiLETA-DRC (DD1HDA)
06	LB(6,0)	26[8]	LB-SUMC	06	DD1-HiLETB-DRC (DD1HDB)
07[1]	LB(7-8,0)	27[9]	LB-SUM4	07	DD2-LoLET-Flux (DD2LF)
08	LB(0,1)	28[10]	LB-SUM5	08	DD2-HiLETA-Flux (DD2HFA)
09	LB(1,1)	29	LB(5,1)	09	DD2-HiLETB-Flux (DD2HFB)
10	LB(2,1)	30	LB(5,2)	10	DD2-LoLET-DRC (DD2LD)
11	LB(3,1)	31	LB(5,3)	11	DD2-HiLETA-DRC (DD2HDA)
12	LB(4,1)	32	LB(0,2)	12	DD2-HiLETB-DRC (DD2HDB)
13	LB(1,2)	33	LB(0,3)		
14	LB(2,2)	34	LB(1,4)		
15	LB(3,2)	35	LB(2,4)		
16	LB(4,2)	36	LB(2,5)		
17[2]	LB(1,3)	37[11]	LB(6,1)		
18[2]	LB(2,3)	38[11]	LB(7,1)		
19	LB(3,3)	39[11]	LB(8,1)		
20	LB(4,3)	40[11]	LB(6,2)		
		41[11]	LB(7,2)		
		42[11]	LB(8,2)		
		43[11]	LB(6,3)		
		44[11]	LB(7,3)		
		45[11]	LB(8,3)		

Notes
1. LB(7-8,0) = LB-B32 = LB(7,0+(8,0)
2. CEASE-II position 17 is the sum of LB(1,3) and LB(2,3); position 18 is vacant
3. LB-SUMA = LB-B46 = LB (4,4)+(4,5)+(3,4)
4. LB-SUM1 = LB (6,1)+(7,1)+(8,1)+(6,2)+(7,2)+(8,2)+(6,3)+(7,3)+(8,3)
5. LB-SUM2 = LB (6,4)+(7,4)+(8,4)+(6,5)+(7,5)+(8,5)+(6,6)+(7,6)+(6,7)+(7,7)+(6,8)+(7,8)
6. LB-SUMB = LB-B49 = LB (8,6)+(8,7)+(8,8)
7. LB-SUM3 = LB (5,4)+(5,5)+(5,6)+(5,7)+(5,8)
8. LB-SUMC = LB-B51 = LB (4,6)+(4,7)+(4,8)
9. LB-SUM4 = LB (3,5)+(3,6)+(3,7)+3,8)
10. LB-SUM5 = LB (0,4)+(0,5)+(0,6)+(0,7)
11. Logic Blocks numbered 37-45 are in CEASE-II telemetry only

13

APPENDIX B – TELESCOPE SUMMED CHANNEL DEFINITION

Primary Channel	T1	T2	T3	T4
LB(1,0) – 1	X			
LB(2,0) - 2	X			
LB(3,0) – 3	X	X		
LB(4,0) – 4	X	X		
LB(1,1) – 9	X	X		
LB(2,1) – 10	X	X		
LB(3,1) – 11	X	X		
LB(4,1) – 12	X	X	X	
LB(1,2) – 13	X	X	X	
LB(2,2) – 14	X	X	X	
LB(3,2) – 15	X	X	X	
LB(4,2) – 16	X	X	X	
LB(1,3) – 17	X	X	X	X
LB(2,3) – 18	X	X	X	X
LB(3,3) – 19	X	X	X	X
LB(4,3) – 20	X	X	X	X

15

APPENDIX C.1 – CEASE SN02 (TSX-5) GEOMETRIC FACTORS

Std Ch	Channel Description	Electrons (Eo = 0.3; 0.2-0.5 MeV)		Protons (n = 2; 2-4)	
		E_T (MeV) Ave (std dev)	G (cm^2 sr) Ave (std dev)	E_T (MeV)	G (cm^2 sr)
D01	DD1LF (mBTA)	1.23	3.54e-1	>30	N/A
	(BTA)	1.51 (0.07)	9.18e-1 (1.87e-1)	>30	N/A
D02	DD2LF	N/A	N/A	>40	N/A
		2.42 (0.29)	6.59e-2 (5.11e-2)	>40	N/A
D03	DD1HFA	1.65	3.01e-2	30.7	1.65e0
		1.88 (0.04)	6.66e-2 (8.31e-3)	26.3 (1.46)	1.32e0 (1.55e-1)
D04	DD2HFA	2.42	4.84e-4	49.3	1.50e0
		3.16 (0.34)	8.78e-3 (7.16e-3)	40.4 (3.4)	1.10e0 (2.02e-1)
D05	DD1HFB	6.46	N/A	21.6	6.66e-1
		6.57 (0.01)	1.45e-3 (2.42e-5)	16.4 (1.9)	5.16e-1 (1.29e-1)
D06	DD2HFB	7.41	N/A	39.6	3.30e-1
		7.60 (0.04)	6.02e-4 (6.02e-5)	28.9 (3.4)	2.30e-1 (5.86e-2)
D07	DD1LF + DD1HFA	1.23	3.65e-1	32.0	2.41e0
		1.51 (0.08)	9.64e-1 (2.00e-1)	29.5 (0.15)	1.98e0 (2.14e-2)
D08	DD2LF + DD2HFA	N/A	N/A , 5.35e-2	52.3	2.60e0
		2.43 (0.29)	6.94e-2 (5.46e-2)	47.5 (1.27)	1.99e0 (1.12e-1)
T01	16 ch sum	0.11	9.86e-4	>1	N/A
		0.14 (0.04)	1.11e-3 (1.33e-4)		
T02	14 ch sum	0.15	7.81e-4	>1	N/A
		0.17 (0.04)	8.15e-4 (8.62e-5)		
T03	9 ch sum	0.35	4.70e-4	81.8	7.13e-1
		0.42 (0.06)	6.05e-4 (1.01e-4)	71.8 (2.44)	4.66e-1
T04	4 ch sum	0.57	2.74e-4	79.2	5.74e-1
		0.56 (0.03)	2.62e-4 (2.22e-5)	67.6 (4.0)	3.77e-1 (4.72e-2)
T05	LBSUM3	N/A	N/A	22.3	2.42e-2
				16.3 (0.6)	1.68e-2 (1.26e-3)
T06	LBSUMA	>4.5	N/A	37.5	1.26e-1
				31.1 (2.4)	9.68e-2 (1.58e-2)
T08	LB(3,3)	0.68	2.07e-5	96.6	4.14e-1
		0.72 (0.06)	2.38e-5 (3.73e-6)	77.0 (7.2)	2.41e-1 (4.85e-2)
T09	LB(4,3)	0.83	6.92e-6	65.6	1.46e-1
		0.90 (0.10)	9.15e-6 (2.45e-6)	52.3 (4.9)	9.74e-2 (1.96e-2)

17

APPENDIX C.2 – CEASE SN07 (DSP21) GEOMETRIC FACTORS

Std Ch	Channel Description	Electrons (Eo = 0.3; 0.2-0.5 MeV)		Protons (power n = 2; 2-4)	
		E_T (MeV)	G (cm^2 sr)	E_T (MeV)	G (cm^2 sr)
D01	DD1LF(mBTA)	1.23	3.61e-1	>30	N/A
	(BTA)	1.51 (0.07)	9.42e-1 (1.92e-1)	>30	N/A
D02	DD2LF	N/A	N/A	>40	N/A
		2.42 (0.29)	6.76e-2 (5.26e-2)	>40	N/A
D03	DD1HFA	1.78	1.81e-2	30.3	1.46e0
		2.02 (0.05)	3.97e-2 (5.02e-3)	25.5 (1.70)	1.16e0 (1.66e-1)
D04	DD2HFA	2.82	5.28e-4	48.5	1.27e0
		3.53 (0.26)	7.77e-3 (4.96e-3)	38.8 (3.62)	9.14e-1 (1.84e-1)
D05	DD1HFB	6.46	N/A	21.6	6.66e-1
		6.57 (0.01)	N/A	16.4 (1.89)	5.16e-1 (1.29e-1)
D06	DD2HFB	6.54	N/A	39.6	3.30e-1
		6.71 (0.12)	N/A	28.9 (3.39)	2.30e-1 (5.86e-2)
D07	DD1LF + DD1HFA	1.23	3.65e-1	32.0	2.41e0
		1.51 (0.08)	9.64e-1 (2.00e-1)	29.5 (0.15)	1.98e0 (2.14e-2)
D08	DD2LF + DD2HFA	N/A	N/A	52.3	2.60e0
		2.43 (0.29)	6.94e-2 (5.46e-2)	47.5 (1.27)	1.99e0 (1.12e-1)
T01	16 ch sum	0.11	9.85e-4	>1	N/A
		0.14 (0.04)	1.11e-3 (1.34e-4)		
T02	14 ch sum	0.15	7.81e-4	>1	N/A
		0.17 (0.04)	8.15e-4 (8.65e-5)		
T03	9 ch sum	0.35	4.16e-4	65.2	6.65e-1
		0.37 (0.03)	4.32e-4 (3.71e-5)	58.7 (0.9)	4.73e-1 (1.49e-2)
T04	4 ch sum	0.58	1.59e-4	60.5	4.45e-1
		0.56 (0.04)	1.49e-4 (1.38e-5)	52.1 (3.1)	3.20e-1 (4.11e-2)
T05	LBSUM3	N/A	N/A	22.6	2.72e-2
				16.7 (0.6)	1.90e-2 (1.50e-3)
T06	LBSUMA	>4.5	N/A	35.1	6.29e-2
				28.5 (2.3)	4.80e-2 (8.39e-4)
T08	LB(3,3)	0.66	1.21e-5	92.6	3.27e-1
		0.70 (0.07)	1.36e-5 (2.43e-6)	71.9 (7.4)	1.90e-1 (4.23e-2)
T09	LB(4,3)	0.83	4.40e-6	53.5	2.08e-1
		0.93 (0.10)	6.45e-6 (1.85e-6)	43.7 (3.9)	1.50e-1 (2.85e-2)

18

APPENDIX C.3 – CEASE SN04 (DSX) GEOMETRIC FACTORS

Std Ch	Channel Description	Electrons (Eo = 0.3; 0.2-0.5 MeV)		Protons (power n = 2; 2-4)	
		E_T (MeV)	G (cm^2 sr)	E_T (MeV)	G (cm^2 sr)
D01	DD1LF(mBTA)	1.23	3.61e-1	>30	N/A
	(BTA)	1.51 (0.07)	9.42e-1 (1.92e-1)	>30	N/A
D02	DD2LF	N/A	N/A	>40	N/A
		2.42 (0.29)	6.76e-2 (5.26e-2)	>40	N/A
D03	DD1HFA	1.78	1.81e-2	30.3	1.46e0
		2.02 (0.05)	3.97e-2 (5.02e-3)	25.5 (1.70)	1.16e0 (1.66e-1)
D04	DD2HFA	2.82	5.28e-4	48.5	1.27e0
		3.53 (0.26)	7.77e-3 (4.96e-3)	38.8 (3.62)	9.14e-1 (1.84e-1)
D05	DD1HFB	6.46	N/A	21.6	6.66e-1
		6.57 (0.01)	N/A	16.4 (1.89)	5.16e-1 (1.29e-1)
D06	DD2HFB	6.54	N/A	39.6	3.30e-1
		6.71 (0.12)	N/A	28.9 (3.39)	2.30e-1 (5.86e-2)
D07	DD1LF + DD1HFA	1.23	3.65e-1	32.0	2.41e0
		1.51 (0.08)	9.64e-1 (2.00e-1)	29.5 (0.15)	1.98e0 (2.14e-2)
D08	DD2LF + DD2HFA	N/A	N/A	52.3	2.60e0
		2.43 (0.29)	6.94e-2 (5.46e-2)	47.5 (1.27)	1.99e0 (1.12e-1)
T01	16 ch sum	0.11	1.22e-3	>1	N/A
		0.13 (0.01)	1.29e-3 (4.69e-5)		
T02	14 ch sum	0.16	9.57e-4	>1	N/A
		0.17 (0.01)	9.77e-4 (3.60e-5)		
T03	9 ch sum	0.37	5.44e-4	78.6	6.15e-1
		0.35 (0.01)	5.07e-4 (7.17e-6)	69.1 (1.7)	4.06e-1 (2.16e-2)
T04	4 ch sum	0.59	1.94e-4	72.2	3.89e-1
		0.53 (0.01)	1.58e-4 (6.36e-6)	60.7 (4.1)	2.61e-1 (3.75e-2)
T05	LBSUM3	N/A	N/A	25.3	1.20e-2
				19.0 (1.2)	7.90e-3 (1.03e-3)
T06	LBSUMA	>9	N/A	42.6	4.38e-2
				34.4 (2.4)	3.20e-2 (4.70e-3)
T08	LB(3,3)	0.68	1.28e-5	101.8	2.84e-1
		0.64 (0.01)	1.09e-5 (4.15e-7)	78.7 (8.2)	1.58e-1 (3.56e-2)
T09	LB(4,3)	0.87	4.80e-6	62.9	1.64e-1
		0.84 (0.01)	4.27e-6 (1.48e-7)	50.8 (4.6)	1.12e-1 (2.18e-2)

APPENDIX D.1 – CRRES SPECTRAL ANALYSIS (PROTONS)

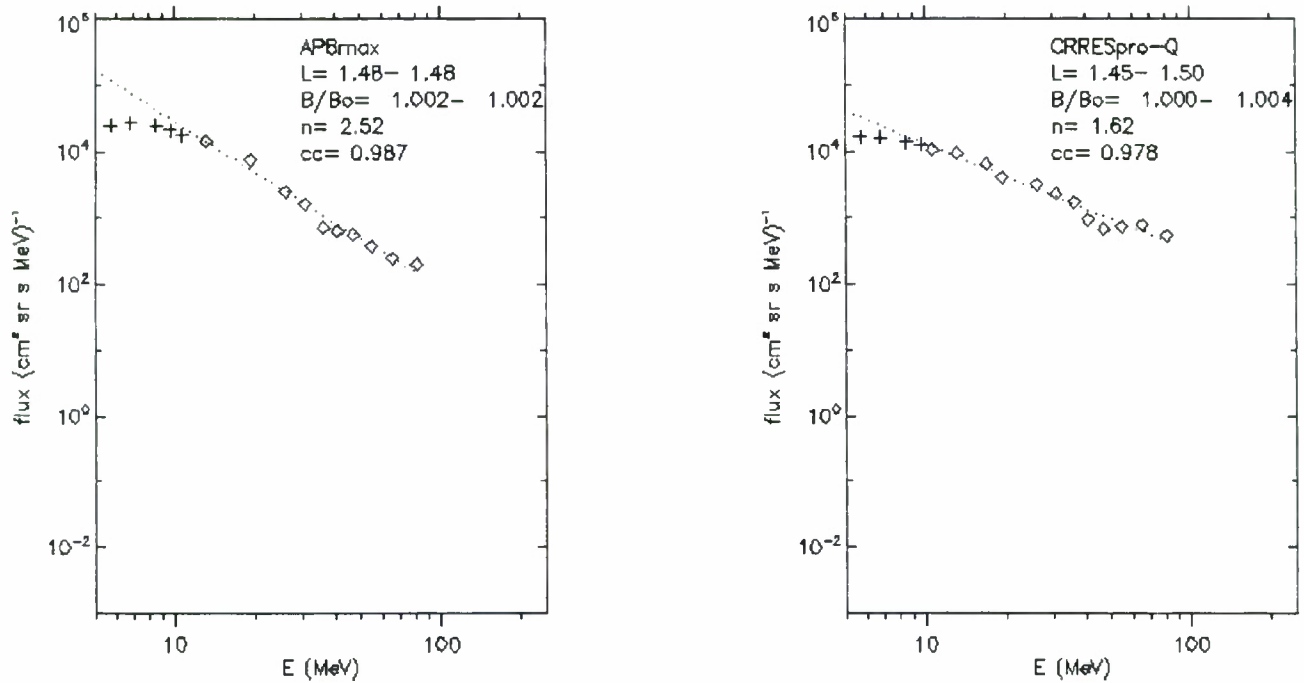Fig. 6 – Shown are proton spectra from AP8max (left) and CRRESPRO-Quiet (right) for L ~ 1.5. The spectra are fit to a power law over the range 10 to 100 MeV and the fitted power law index (n) is provided in the legend.
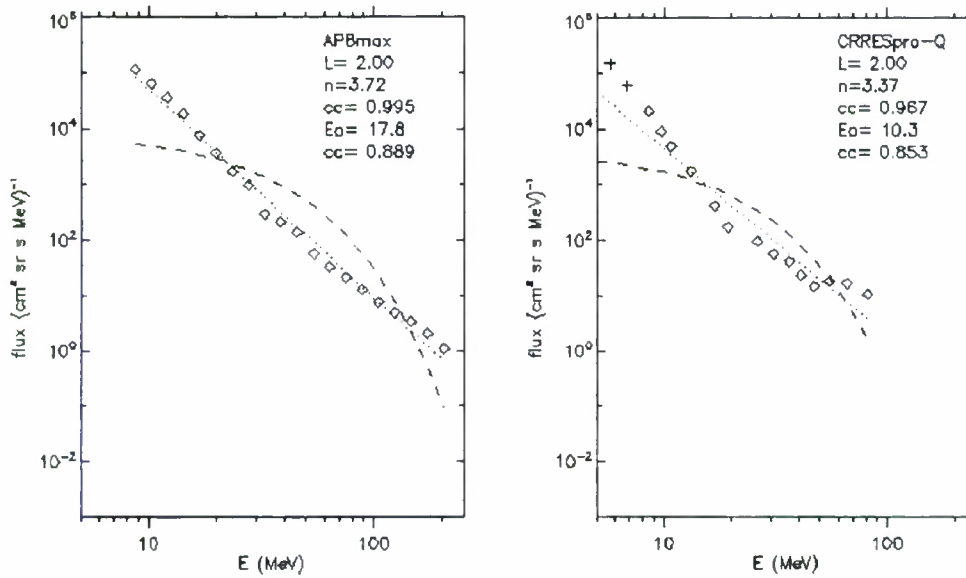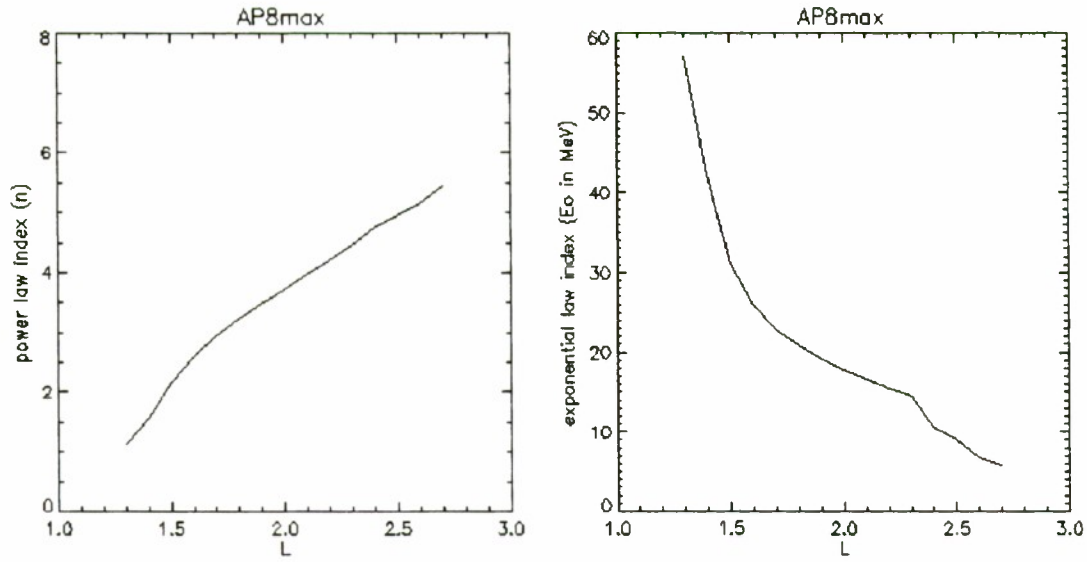

Fig. 7 – Shown are proton spectra from AP8max (left) and CRRESPRO-Quiet (right) for L ~ 2. The spectra are fit to a power law over the range 10 to 100 MeV and the fitted power law index (n) is provided in the legend.

Fig. 8 – Shown are the computed proton (from AP8max model) power law index (left) and exponential index (right) plotted versus L.
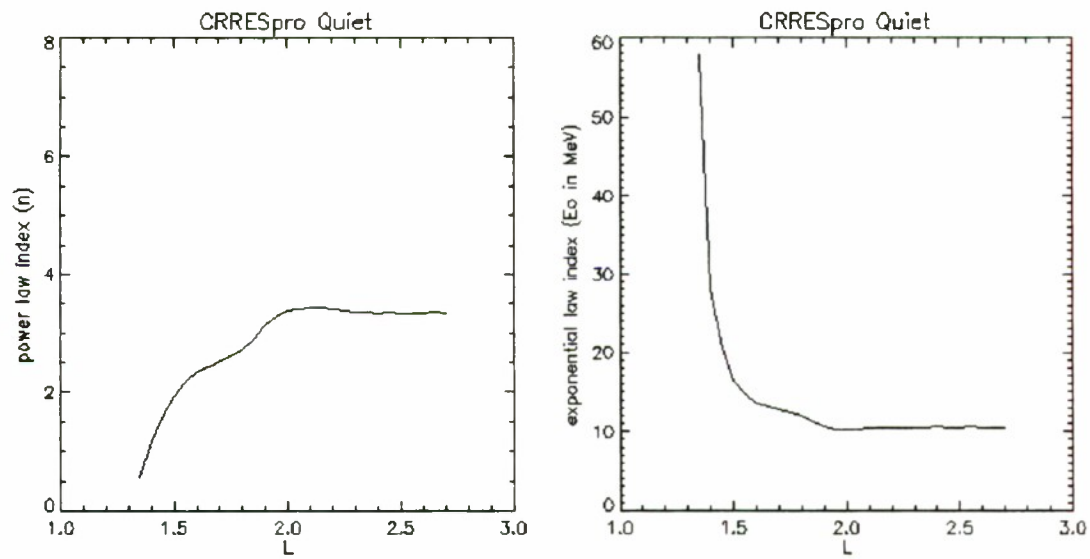

Fig. 9 – Shown are the computed proton (from CRRESpro-Quiet model) power law index (left) and exponential index (right) plotted versus L.

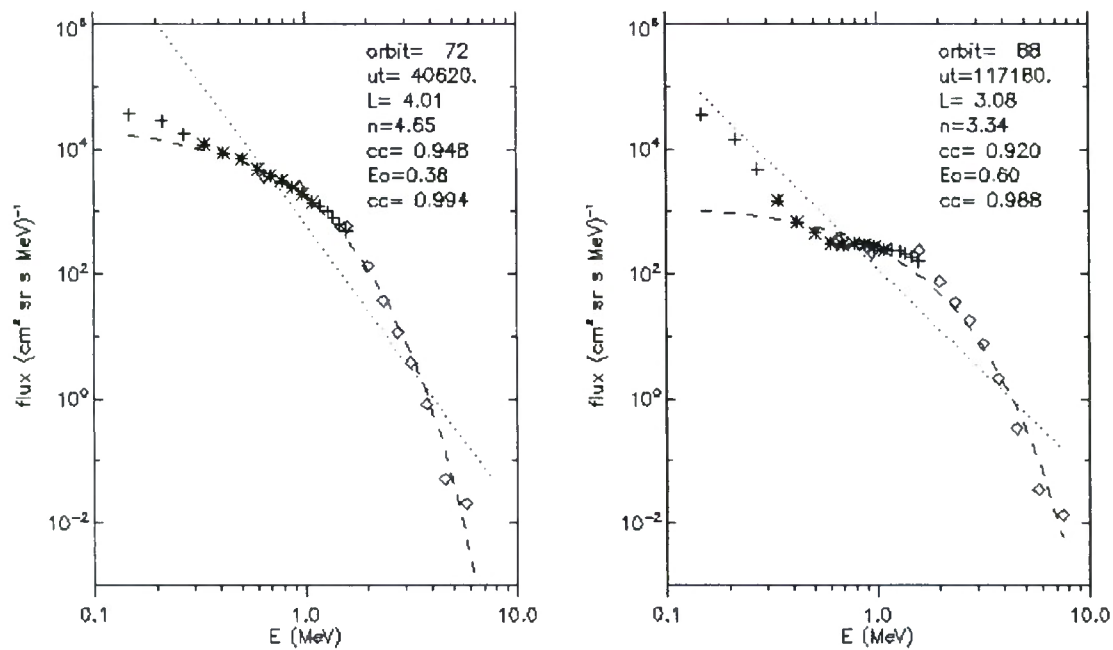# APPENDIX D.2 – CRRES SPECTRAL ANALYSIS (ELECTRONS)

Fig. 10 – Shown are CRRES electron spectra from orbit 72, L ~ 4.0 (left) and orbit 88, L ~ 3.0 (right). The spectra are fit to a power law (dotted line) and exponential (dashed line), with the fitted power law (n) and exponential (E_o) indices provided in the legend.
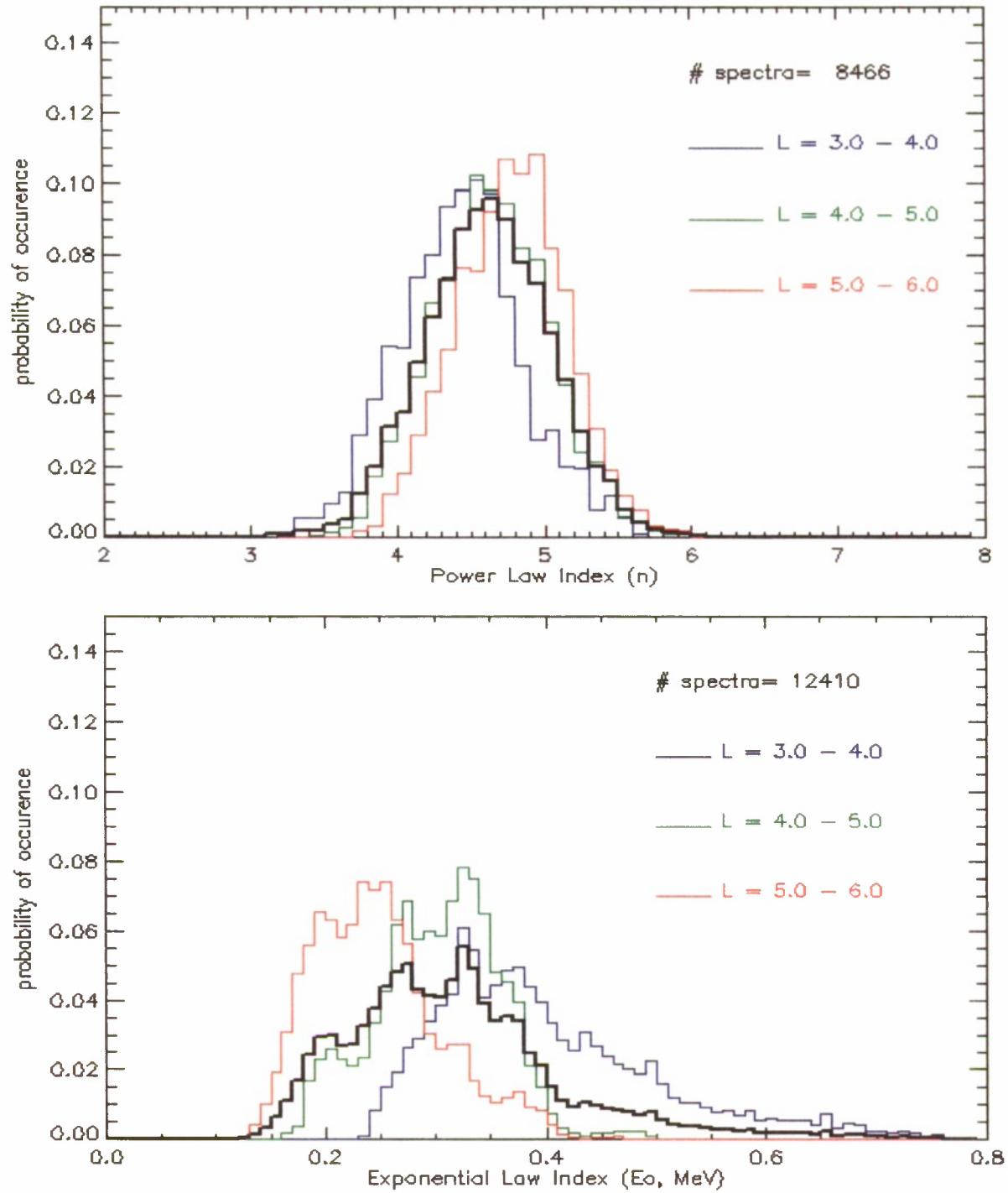
Fig 11. – Histograms showing the frequency of occurrence for a range of power law indices (top) and exponential indices (bottom) computed from CRRES electron spectra, for three different L ranges (shown in legend).